Ceramic Genome, Computational Modeling, and Design

DESIGN OF NEW GRADIENT CEMENTED CARBIDES AND HARD COATINGS THROUGH CERAMIC GENOME

Weibin Zhang[a], Yong Du[a,*], Li Chen[a], Yingbiao Peng[a], Peng Zhou[a], Weimin Chen[a], Kaiming Cheng[a], Lijun Zhang[a], Wen Xie[b], Guanghua Wen[b], and Shequan Wang[b]
[a] State Key Lab of Powder Metallurgy, Central South University, Hunan, 410083, China
[b] Zhuzhou cemented carbide cutting tools limited company, Zhuzhou, Hunan, 412007, China

ABSTRACT

The concept of ceramic genome is briefly introduced, and its combination with CALPHAD (CALculation of PHAse Diagrams) method is a powerful tool for materials process optimization and alloy design. The quality of CALPHAD-type calculations is strongly dependent on the quality of the thermodynamic and diffusivity databases. The development of thermodynamic and diffusivity databases for cemented carbides is described. Several gradient cemented carbides sintered under vacuum and various partial pressures of N_2 have been studied via experiment and simulation. Examples of ceramic genome applications in design and manufacture for different kinds of cemented carbides are shown using the databases and comparing where possible against experimental data, thereby validating their accuracies. Metastable Ti-Al-N coatings have been well acknowledged as protective layer for industrial applications due to their excellent mechanical, chemical and thermal properties. Here, we study the effect of Zr addition on structure and thermal properties of $Ti_{1-x}Al_xN$ based coatings under the guidance of ab initio calculations. The preparation of $Ti_{1-x-z}Al_xZr_zN$ by magnetron sputtering verifies the suggested cubic (NaCl-type) structure for x below 0.6–0.7 and $z \leq 0.4$. Alloying with Zr also promotes the formation of cubic domains but retards the formation of stable wurtzite AlN during thermal annealing.

INTRODUCTION

Cemented carbides have long been used in applications such as cutting, grinding, and drilling[1]. Cemented carbides[2] are hard and tough tool materials consisting of micrometer-sized tungsten carbide embedded in a metal binder phase, usually rich in Co. Cubic carbides or carbonitrides based on Ta, Ti, and Nb are often added in cemented carbides to increase the resistance to plastic deformation or as gradient formers[1]. Some grain growth inhibitors such as Cr and V may also be added in small amounts. In order to increase cutting performance of the cemented carbide inserts, the wear surface are usually coated with a thin layer of hard material[3]. Due to the high deposition temperature and a large difference in thermal expansion coefficients between the coating and substrate, cracks would be introduced into the coating unavoidably[4]. And the formed cracks might easily propagate into the substrate to cause failure when coating tools are employed in metal machining[5]. In order to prevent crack propagation from the coating into the substrate, a gradient layer, which is free of cubic phases and enriched in binder phase, is introduced between coating and substrate[5].

In the past decades, cemented carbides were mainly developed through a large degree of testing. However, there are numerous factors influencing the microstructure and properties of cemented carbides, such as alloy composition, sintering temperature, time and partial pressure and so on. These factors can only be varied in an infinite number of ways through experimental method. In order to shorten

development time, reduce the cost and improve outcome, the concept of materials genome has been proposed. Computation, experimentation, and database are identified as three major components of materials genome. The ceramic genome can describe the interaction of the various process conditions, which presents the opportunity to design and produce new kinds of cemented carbides more efficiently. CALPHAD (CALculation of PHAse Diagrams) method is a powerful tool to establish the database of various properties in the ceramic genome. Computational thermodynamics, using, e.g. the Thermo-Calc and DICTRA packages, has shown to be a powerful tool for processing advanced materials in cemented carbides, which is more efficient on composition and process parameters optimization compared with expensive and time consuming experimental methods. With the development of thermodynamic and diffusivity databases, it is possible to make technical calculations on commercial products which are multicomponent alloys. On the basis of thermodynamic database, thermodynamic calculations can give an easy access to what phases form at different temperatures and alloy concentrations during the manufacture process. By combining CSUTDCC1 and CSUDDCC1 databases, DICTRA[6] permits simulations of the gradient process, which is a major advance in the understanding of the gradient zone formation in the cemented carbides.

Ti-Al-N hard coatings with cubic (c) NaCl structure, where Al substitutes for Ti in the TiN-based structure (i.e., c-$Ti_{1-x}Al_xN$), are widely used in cutting tools because of their high hardness and wear resistance as well as good thermal properties[7]. Because of the spinodal decomposition of c-$Ti_{1-x}Al_xN$ into nano-size cubic Ti-rich and Al-rich domains at elevated temperatures, the age-hardening abilities of Ti-Al-N coatings can improve the mechanical properties of coatings[8]. Due to solid solution strengthening, alloying Zr to Ti-Al-N coating can improve the hardness. Unfortunately, a huge amount of work is needed to find appropriate elements by using experimental method, while first-principles calculations on the investigation of structural and mechanical properties can reduce the workload effectively and provide the reasonable explanation for the experimental observation.

This paper is devoted to 1) describe the development of the thermodynamic and diffusion databases in cemented carbides, 2) design experiments to investigate the gradient zone formation under different sintering environments, 3) validate the accuracy and reliability of the presently established databases in ceramic genome by comparing the experimental and simulation results, 4)investigate the structural and thermal properties of Ti-Al-Zr-N hard coatings by first-principles calculations and experiment, and 5) present the schematical ceramic genome strategy for the development of new cemented carbides and hard coating.

ESTABLISHMENT OF THE CERAMIC GENOME

Development of Thermodynamic and Diffusivity Databases

The development of thermodynamic and diffusivity databases in cemented carbides has started from the major elements in gradient cemented carbides C-Co-Cr-W-Ta-Ti-Nb-N. The usage of ceramic genome in industry will necessarily require that thermodynamic and diffusivity databases provide data that is not only of high quality, but relevant to industrially complex materials.

Developed using the CALPHAD approach, the thermodynamic database, CSUTDCC1, is based on critical evaluations of binary, ternary and even higher order systems which enable making predictions

for multicomponent systems and alloys of industrial importance. Six important phases in cemented carbides, e.g. liquid, WC, carbides or carbonitrides, binder (Co), and eta (M_6C or $M_{12}C$) phases, are the main focus during the modeling. A large number of additional phases are also included in CSUTDCC1, because many of the binary and ternary systems in CSUTDCC1 have been assessed over their entire composition and temperature ranges. It is important to have reliable descriptions for all the stable phases in the system when developing new alloys and exploring new composition ranges. The thermodynamic models describe the thermodynamic properties of various types of phases depending on the crystallography, order-disorder transitions, and magnetic properties of the phases. With parameters stored in database, many different models[9], including the substitution solution model, sublattice model, order-disorder model, have been adopted for the phases in cemented carbide systems. The thermodynamic models for Gibbs energy of a phase can be represented by a general equation:

$$G_m^\theta = {}^{ref}G_m^\theta + {}^{id}G_m^\theta + {}^{E}G_m^\theta + {}^{magn}G_m^\theta \quad (1)$$

Here ${}^{ref}G_m^\theta$ represents the Gibbs energy of the pure elements of the phase and ${}^{id}G_m^\theta$ represents the contribution due to the ideal mixing. The term ${}^{E}G_m^\theta$ represents the excess energy and ${}^{magn}G_m^\theta$ the magnetic contribution.

In contrast to extensive efforts on the establishment of thermodynamic database for multicomponent cemented carbides, diffusivities in the multicomponent cemented carbides have received limited investigations both experimentally and theoretically. In a multicomponent system, a large number of diffusivities need to be evaluated, making a database very complex. A superior alternative is to model atomic mobility instead. In this way, the number of the stored parameters in the database is substantially reduced and the parameters are independent. A detailed description for the atomic mobility is given by Andersson and Ågren[10]. The atomic mobility for an element B, M_B, can be expressed as

$$M_B = M_B^0 \exp(-Q_B/RT)(1/RT) \quad (2)$$

where R is the gas constant, T the temperature, M_B^0 a frequency factor and Q_B the activation enthalpy. Both M_B^0 and Q_B are in general dependent on composition and temperature.

The simulation of gradient zone formation is based on the model for long-range diffusion occurring in a continuous matrix with dispersed phases. Due to the presence of dispersed phases (WC, carbides and carbonitrides), the diffusion is reduced in the matrix (the liquid binder phase)[11]. A so-called labyrinth factor $\lambda(f)$, where f is the volume fraction of the matrix, was introduced to reduce the diffusion coefficient matrix.

$$D_{kj,eff}^n = \lambda(f) D_{kj}^n \quad (3)$$

First-principles Calculations of Hard Coatings

First-principles calculation is one of the theoretical methods to study the microstructure and

properties of materials. This method is based on the density functional theory (DFT) with the local density approximation (LDA)[12] or generalized gradient approximation (GGA)[13]. In the present work, first-principles calculations are performed by Vienna ab-initio simulation package (VASP)[14]. The electron-ion interactions are described by the projector augmented wave (PAW) method[15], and the exchange-correlation is depicted by GGA and LDA. The energy cutoff of the wave functions is taken as 1.3 times higher than the default values in the psudopotentials. The Monkhorst-Pack scheme[16] of k-points sampling and the linear tetrahedron method including Blöchl corrections[17] are adopted for the integration in the Brillouin zone. The total number of k-points is at least 10,000 per reciprocal atom for all the calculations. The convergence criterion for electronic self-consistency is 10^{-6} eV per unit cell.

The quasiharmonic approach is adopted to evaluate the finite-temperature Helmholtz energy as a function of volume V and temperature T[18]

$$F(V,T) = E(V) + F_{vib}(V,T) + F_{ele}(V,T) \quad (4)$$

where $E(V)$ is the static energy at 0 K without the zero-point vibrational energy, $F_{vib}(V,T)$ is the vibrational contribution to Helmholtz energy with the input of phonon density of state (DOS), and $F_{ele}(V,T)$ is the thermal electronic contribution to the free energy, which can be calculated by Mermin statistics[19] with input of electronic DOS from first-principles directly.

EXPERIMENTAL

The alloys were prepared from a powder mixture of WC, (Ti,W)C, Ti(C,N), and metallic Co powder provided by Zhuzhou cemented carbide cutting tools limited company. The composition of the sintered material is given in Table I. After milling and drying, the powders were pressed into cutting tool inserts. Samples were dewaxed and sintered under different nitrogen partial pressures (0, 20 and 40 mbar) at 1723 K for 1 h. After sintering the samples were cut, embedded in resin and polished. SEM (Nova NanoSEM 230, USA) was employed to investigate the microstructure of the gradient zone, and EPMA (JXA-8230, JEPL, Japan) was used to determine the concentration profiles of the elements.

Table I. Chemical composition of the investigated cemented carbides (wt%)

Alloy	Ti	Co	C	N	W
WC-Ti(C,N)-Co	5	7.5	6.35	0.1	Bal.

$Ti_{1-x-z}Al_xZr_zN$ films were deposited onto several substrates by unbalanced magnetron sputteringin a mixed Ar+N_2 (both of 99.999% purity) glow discharge. DSC with TGA was performed in a Netzch-STA 409C from room temperature (RT) to 1500 °C with a heating rate of 20 K/min in flowing He (99.9% purity, 20 sccm flow rate) .The chemical compositions of the films were determined using energy dispersive X-ray analysis (EDX) with an Oxford Instruments INCA EDX. Phase identification and structural investigations of the layers in their as deposited state and after thermal treatment with the DSC equipment in He or synthetic air were conducted by XRD with CuK_α radiation using a Brucker D8 diffractometer in Bragg/Brentano mode. DFT calculations were performed using the VASP code.

RESULTS AND DISCUSSION

Verification and Application of the Databases

It is generally known that the graphite and eta (M_6C or $M_{12}C$) phases are unexpected phases and the carbon content in cemented carbides should be carefully controlled to avoid the formation of these phases. With the aid of thermodynamic calculations, it is easy to see how to control the carbon content and how the carbon content affects the choice of sintering temperature when developing a new alloy. Figure 1(a) shows a calculated phase equilibria closing to the sintering region of an alloy with the composition of C-W-9Co-15Ti-10Ta-2Nb-0.1N (wt.%). As can be seen, the carbon content have to be carefully located in a narrow range about 0.2 wt.% in order to avoid the appearance of unwanted phases. Figure 1(b) presents a similar calculation by adding 2 wt.%, of Cr. From Fig. 1(b), it can be seen that the melting point of binder phase is decreased substantially by Cr addition and the existence of the preferable fcc_Co + $M(C, N)_x$ + WC equilibrium is broadened. On the basis of CSUTDCC1, a similar calculation can be performed on alloys with any composition, which will be a useful guidance for developing new alloys.

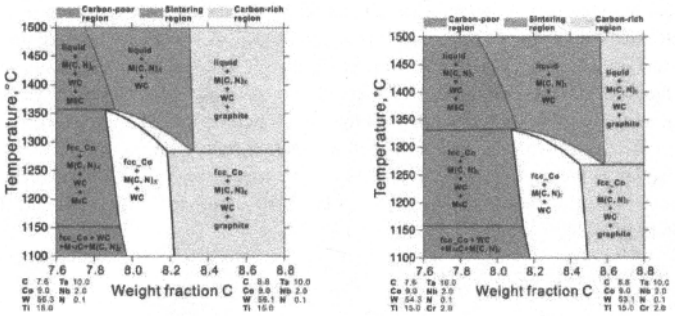

Figure 1. Calculated phase equilibria closing to the sintering region of alloys with the composition of (a) C-W-9Co-15Ti-10Ta-2Nb-0.1N (wt.%) and (b) C-W-2Cr-9Co-15Ti-10Ta-2Nb-0.1N (wt.%)

Study of Gradient Zone Formation in Cemented Carbides

Figure 2 shows SEM micrograph of the cross section of alloys sintered under different nitrogen partial pressures (0, 20 and 40 mbar) at 1450 ℃ for 1 h. It is obvious that the near-surface of the alloy has formed the gradient zone which is enriched in binder phase and depleted in cubic carbides. Comparing the micrographs of the cross section of the cemented carbides sintered under different low nitrogen gas pressure shows that a decreasing thickness of gradient layer with increasing nitrogen gas pressure.

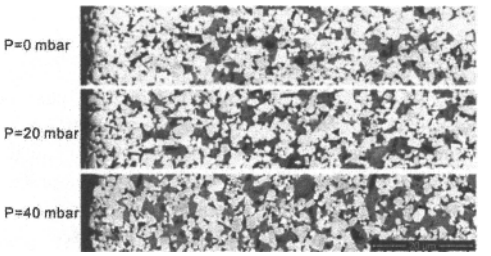

Figure 2. SEM micrograph of the cross section of alloys sintered under different nitrogen partial pressures (0, 20 and 40 mbar) at 1450 ℃ for 1 h.

By combining the presently established thermodynamic and diffusivity databases, DICTRA software has been used to simulate the formation of the gradient zone. Figures 3(a)-(b) illustrate the simulated elemental concentration profiles for Co and Ti in alloys after sintering for 1 h at 1450 ℃ under different nitrogen partial pressures (0, 20 and 40 mbar), compared with the measured data. This result indicates that the content of Ti is free in the near-surface zone and enrich inside the surface zone. At the near-surface zone, the content of Co increases sharply and reached a maximum value. Beneath the near-surface zone, a decrease of Co is observed, which leads to the minimum value. Above this minimum value, the content of Co increases slowly to its bulk value. The calculated thickness of the gradient layer decreases with the increasing of nitrogen partial pressure, which shows the similar diffusion behavior as the experimental results. As can be seen in Figs. 3(a)-(b), the presently obtained thermodynamic and diffusion databases can reasonably reproduce most of the experimental concentration profiles.

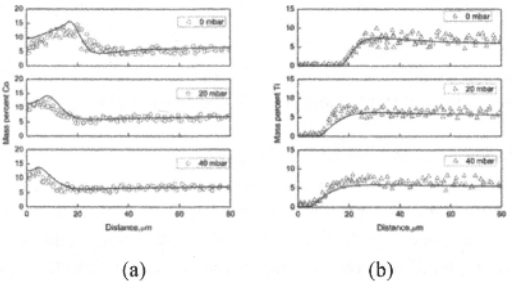

(a) (b)

Figure 3. Concentration profile for (a) Co and (b) Ti in alloys: measurement (symbols) and calculation (curve).

Ti-Al-Zr-N Hard Coatings

Elemental analysis by EDX reveals that our $Ti_{1-x-z}Al_xZr_zN$ films are stoichiometric with N/metal ratios of 1±0.1and compositions of $Ti_{0.48}Al_{0.52}N$, $Ti_{0.40}Al_{0.55}Zr_{0.05}N$, $Ti_{0.39}Al_{0.51}Zr_{0.10}N$, $Ti_{0.36}Al_{0.47}Zr_{0.17}N$, and $Ti_{0.34}Al_{0.37}Zr_{0.29}N$, respectively. XRD investigations in Fig. 4 reveal a single phase cubic structure,

which is in agreement with ab intio calculations. Figure 5a presents the energy of formation (E_f) of the cubic and wurtzite $Ti_{1-x-z}Al_xZr_zN$ alloys with constant z = 0, 0.05 and 0.1 as a function of the AlN mole fraction x. The data suggest a transition from cubic to wurtzite structure $Ti_{1-x-z}Al_xZr_zN$ at x ~0.72, 0.70, and 0.68 for a ZrN mole fraction z of 0, 0.05, and 0.10, respectively. Since the compositional steps given by the supercell sizes are different for the cubic (1/18) and for the wurtzite (1/16) alloys, to evaluate the maximum solubility of AlN in the cubic phase we proceeded as follows. First, we fitted each set of data with constant ZrN mole fraction with a quadratic polynomial ($a_0 + a_1 \cdot x + a_2 \cdot x^2$). For c-$Ti_{1-x-z}Al_xZr_zN$, the AlN mole fraction x was varied 19 times for z = 0, 12 times for z = 0.055, and 10 times for z = 0.111. The calculations of w-$Ti_{1-x-z}Al_xZr_zN$ were obtained with 7, 6, and 5 variations in x for z = 0, 0.0625, and 0.125, respectively, in the composition range x = 0.5–1. Subsequently, for each phase (i.e. cubic or wurtzite) we fitted individually the coefficients (i.e. a_0, a_1, a_2) of their quadratic polynomial for the three different ZrN mole fractions, z, with a linear expression in the ZrN contents. This way, two polynomial fits (one for the cubic and one for the wurtzite modification) as functions of x (AlN mole fraction) and z (ZrN mole fraction) were obtained. In the last step, we used these fits to estimate the cross-over between the formation energies of the cubic and wurtzite phases at fixed ZrN mole fractions (and thus to estimate the influence of Zr on the maximum AlN mole fraction in the cubic $Ti_{1-x-z}Al_xZr_zN$).

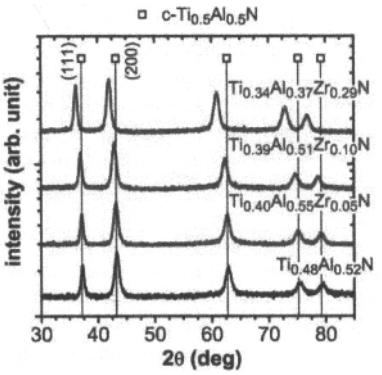

Figure 4. XRD patterns of as deposited powdered $Ti_{1-x-z}Al_xZr_zN$ thin films.

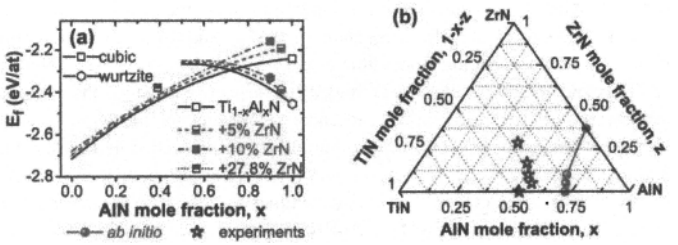

Figure 5. (a) Energy of formation (E_f) for c-$Ti_{0.33}Al_{0.39}Zr_{0.28}N$ and cubic and wurtzite phases $Ti_{1-x-z}Al_xZr_zN$ with z = 0, 0.05 and 0.1 as functions of AlN mole fraction. (b) Overall chemical compositions of our $Ti_{1-x-z}Al_xZr_zN$ films, in the as deposited state, plotted within the TiN–AlN–ZrN quasi-ternary phase diagram. The solid line indicates the transition between preferred cubic and wurtzite phases

Ab initio obtained mixing enthalpies (from the binary constituents c-TiN, c-ZrN, and w-AlN) for c-$Ti_{0.48}Al_{0.52}N$, c-$Ti_{0.4}Al_{0.55}Zr_{0.05}N$, c-$Ti_{0.39}Al_{0.51}Zr_{0.1}N$, and c-$Ti_{0.34}Al_{0.37}Zr_{0.29}N$ are 104, 116, 119, and 120 meV/at, respectively, and hence increase with increasing ZrN content. When using a cubic solid solution between TiN and ZrN, i.e. c-$Ti_{1-y}Zr_yN$ (with $y = z/(1-x)$) as a constituent next to w-AlN, we obtain mixing enthalpies of 104, 98, 87, and 72 meV/at for z = 0, 0.05, 0.10, and 0.29, respectively. The latter reference and the comparison of the mixing enthalpies with the DSC experiments, which exhibit an overall exothermic contribution of 192, 232, 227, and 140 W·K/g for the coatings c-$Ti_{0.48}Al_{0.52}N$, c-$Ti_{0.4}Al_{0.55}Zr_{0.05}N$, c-$Ti_{0.39}Al_{0.51}Zr_{0.1}N$, and c-$Ti_{0.34}Al_{0.37}Zr_{0.29}N$, suggests that there is no separation into the constituents c-TiN, c-ZrN, and w-AlN but into c-$Ti_{1-y}Zr_yN$ and w-AlN. This is verified by XRD analysis of samples annealed to various temperatures using the DSC equipment with the same setup, atmosphere, heating and cooling rates.

Figure 6 shows the structural evolution during annealing of our $Ti_{0.48}Al_{0.52}N$ (a) $Ti_{0.4}Al_{0.55}Zr_{0.05}N$ (b) and $Ti_{0.39}Al_{0.51}Zr_{0.1}N$ (c) films by means of XRD patterns after annealing to 700, 850, 1100, 1200, and 1500 °C. The Zr-free $Ti_{0.48}Al_{0.52}N$ film exhibits a small shift of the XRD reflexes during annealing to 700 °C as compared with the as deposited state, see Fig. 6a, suggesting only minute structural changes like recovery and relaxation which contribute to the exothermic DSC feature in this temperature range. The XRD patterns of the Zr-containing films $Ti_{0.4}Al_{0.55}Zr_{0.05}N$ and $Ti_{0.39}Al_{0.51}Zr_{0.1}N$ annealed to 700 °C reveal also a shift in the peak position to higher diffraction angles but also an increase in peak broadening, see Figs. 6b and c. The latter is an indication for a reduction in grain size and/or an increase in microstresses which can result from the onset of a decomposition process. This can better be seen after annealing at 850 °C, where the XRD reflexes exhibit on both sides (lower and higher diffraction angles) an increase in intensity and width, suggesting the formation of Al-depleted and Al-enriched domains. After annealing at 1100 °C, a pronounced shoulder-formation on both sides of the 'matrix' XRD peak can be seen clearly. These shoulders indicate the formation of TiN- and AlN-rich cubic domains for $Ti_{0.48}Al_{0.52}N$, and TiN-, ZrN- and AlN-rich cubic domains for the Zr-containing films. While the Zr-free film, $Ti_{0.48}Al_{0.52}N$, exhibits the formation of w-AlN already after annealing at 1100 °C, no

w-AlN formation can be detected for the Zr-containing films (compare Figs. 6a, b, and c), indicating that Zr effectively retards the formation of w-AlN. After annealing at 1200 ℃, almost no intensity at the XRD peak positions of as deposited films can be detected, indicating close-to-complete decomposition of the original supersaturated matrix. The $Ti_{0.48}Al_{0.52}N$ film is mainly composed of TiN- and AlN-rich cubic phases and w-AlN, whereas it is still hard to detect any w-AlN for the Zr containing films, $Ti_{0.4}Al_{0.55}Zr_{0.05}N$ and $Ti_{0.39}Al_{0.51}Zr_{0.1}N$, which at this stage compose mainly of ZrN-, TiN- and AlN-rich cubic phases.

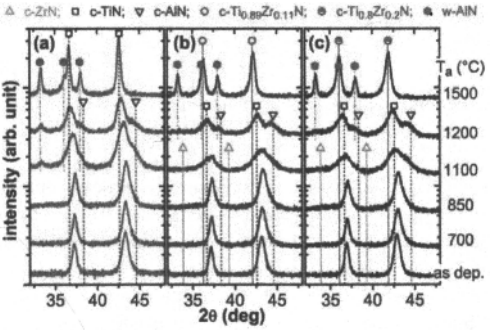

Fig. 6 XRD patterns after annealing in vacuum to temperatures T_a up to 1500 ℃ of (a) $Ti_{0.48}Al_{0.52}N$, (b) $Ti_{0.40}Al_{0.55}Zr_{0.05}N$, and (c) $Ti_{0.39}Al_{0.51}Zr_{0.10}N$.

SCHEMATICAL CERAMIC GENOME

Based on the ceramic genome strategy, several brands of cemented carbides have been developed in the present work, as shown in Fig. 7. The path toward ceramic genome implementation in cemented carbides design and manufacture can be expressed in Fig. 8. Firstly, alloy composition and process parameters are designed via CALPHAD or First-principles calculations. Secondly, the gradient zone formation, microstructure and mechanical properties can be predicted based on the accurate databases. Thirdly, a series of corresponding cemented carbides and hard coatings are prepared under the guidance of the previous steps. After that, the microstructure and mechanical properties of the cemented carbides and hard coatings are investigated experimentally, thereby validating the accuracy of the calculations/simulations. Process routes are optimized and finally chosen for industrial production of cemented carbides with excellent or special performances.

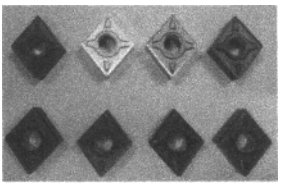

Figure 7. Designed and manufactured industrial cemented carbides with the integration of ICME.

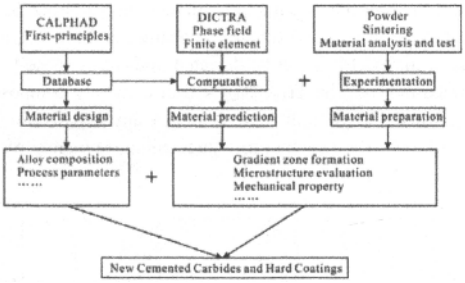

Figure 8. A schematical ceramic genome strategy to develop new gradient carbides and hard coatings.

CONCLUSION

The ceramic genome is a powerful tool for materials process optimization and alloy design. Thermodynamic database and diffusivity database for cemented carbides have been developed through a combination of experimental, theoretical and assessment work. Gradient cemented carbides WC-Ti(C,N)-Co, sintered under various partial pressures of N_2 have been prepared and investigated by means of SEM and EPMA techniques. Good agreements between simulated and measured results indicate the powerful ability of the presently established databases in cemented carbides design and process optimization. The structure and thermal properties are investigated using experimental methods combined with first-principles calculations. Based on the results presented, we can conclude that the coating $Ti_{0.40}Al_{0.55}Zr_{0.05}N$ which contains only 5% Zr at the metal sublattice exhibits the best mechanical and thermal properties. A schematical ceramic genome strategy to develop new gradient carbides and hard coatings is presented.

ACKNOWLEDGEMENT

The financial support from Creative Research Group of National Natural Science Foundation of China (Grant No. 51021063) and Zhuzhou cemented carbide cutting tools limited company of China is acknowledged.

REFERENCES

[1]H. E. Exner, Physical and chemical nature of cemented carbides, *Int. Met. Rev.*, **24** (4), 149-73 (1979).
[2]H.O. Andren, Microstructures of Cemented carbonitrides, *Mater. Des.*, **22** (6), 491-98 (2001).
[3]M. Ekroth, R. Frykholm, M. Lindholm, H.O Andrén, and J. Ågren, Gradient zones in WC-Ti (C, N)-Co-based cemented carbides: experimental study and computer simulations, *Acta Mater.*, **48** (9), 2177-85 (2000).
[4]M. Fitzsimmons and V.K. Sarı, Development of CVD WC-Co coatings, *Surf. Coat. Technol.* **137**, 158-63 (2001).
[5]L. Chen, E.X. Wu, F. Yin, and J. Li, Effects of gradient structure on the microstructures and properties of coated cemented carbides, *J. Univ. Sci.Tech. Beijing*, **13** (4), 363–67 (2006).

[6]J. O. Andersson, L. Hoeglund, B. Jansson, and J. Ågren, Computer simulation of multicomponent diffusional transformations in steel, *Fundam. Appl. Ternary Diffus., Proc. Int. Symp.*, 153-63 (1990).
[7]L. Chen, M. Moser, Y. Du, and P. H. Mayrhofer, Compositional and structural evolution of sputtered Ti-Al-N, *Thin Solid Films*, **517**, 6635-41 (2009).
[8]L. Chen, Y. Du, P. H. Mayrhofer, S. Q. Wang, and J. Li, The influence of age-hardening on turning and milling performance of Ti-Al-N coated inserts, *Surf. Coat. Technol.*, **202** (21), 5158-61 (2008).
[9]N. Saunders, A. P. Miodownik, Calculation of Phase Diagrams (CALPHAD): A Comprehensive Guide, *Elsevier*, New York, 1998.
[10]J.-O. Andersson and J. Ågren, Models for numerical treatment of multicomponent diffusion in simple phases, *J. Appl. Phys.* **72**, 1350-55 (1992).
[11]R. Frykholm, M. Ekroth, B. Jönsson, J. Ågren, and H.O. Andrén, A new labyrinth factor for modelling the effect of binder volume fraction on gradient sintering of cemented carbides, *Acta Mater.*, **51**, 1115-21 (2003).
[12]J. P. Perdew and A. Zunger, Self-interaction correction to density-functional approximations for many-electron systems, *Phys. Rev. B*, **23** (10), 5048-79 (1981).
[13]J. P. Perdew, K. Burke, and M. Ernzerhof, Generalized Gradient Approximation Made Simple, *Phys. Rev. Lett.*, 77 (18), 3865-68 (1996).
[14]G. Kresse and J. Furthmüller, Efficient iterative schemes for ab initio total-energy calculations using a plane-wave basis set, *Phys. Rev. B*, **54** (16), 11169-86 (1996).
[15]P. E. Blöchl, Projector Augmented-Wave Method, *Phys. Rev. B*, **50** (24), 17953-79 (1994).
[16]M. Methfessel and A. T. Paxton, High-precision sampling for Brillouin-zone integration in metals, *Phys. Rev. B*, **40** (6), 3616-21 (1989).
[17]P. E. Blöchl, O. Jepsen, and O. K. Andersen, Improved tetrahedron method for Brillouin-zone integrations, *Phys. Rev. B*, **49**, 16223-33 (1994).
[18]S. L. Shang, Y. Wang, and Z. K. Liu, First-principles calculations of phonon and thermodynamic properties in the born-alkaline earth metal binary systems:B-Ca, B-Sr, and B-Ba, *Phys. Rev. B*, **75**, 024302-12 (2007).
[19]Y. Wang, Z. K. Liu, and L. Q. Chen, Thermodynamic properties of Al, Ni, NiAl, and Ni_3Al from first-principles calculations, *Acta. Mater*, **52**, 2665-71 (2004).
[20]C. K. Gan, Y. P. Feng, and D. J. Srolovitz, First-principles calculation of the thermodynamics of $In_xGa_{1-x}N$ alloys: Effect of lattice vibrations, *Phys. Rev. B*, **73**, 235214-21 (2006).